Chapter 1

Photonic Crystal Ring Resonator Based Optical Filters

S. Robinson and R. Nakkeeran

Additional information is available at the end of the chapter

http://dx.doi.org/10.5772/54533

1. Introduction

Photonic Crystals are periodic nanostructures that are designed to affect the motion of photons in the same way as the periodic potential in a semiconductor crystal affects the electron motion by defining allowed and forbidden electronic energy bands [1, 2]. Generally, PCs are composed of periodic dielectric, metello-dielectric nanostructures, which have alternative lower and higher dielectric constant materials in one, two and/or three dimensions to affect the propagation of electromagnetic waves inside the structure. As a result of this periodicity, the transmission of light is absolutely zero in certain frequency ranges which is called as Photonic Band Gap (PBG).

By introducing the defects (point defects or line defects or both) in these periodic structures, the periodicity and thus the completeness of the PBG are entirely broken which allows to control and manipulate the light [1, 2]. It ensures the localization of light in the PBG region which leads to the design of the PC based optical devices.

2. History of photonic crystals

Electromagnetic wave propagation in periodic media is first studied by Lord Rayleigh in 1888. These structures are One Dimensional (1D) Photonic Crystals (1DPCs) which have a PBG that prohibits the light propagation through the planes. Although PCs have been studied in one form or another since 1887, the term "Photonic Crystal" is first used over 100 years later, after Yablonovitch and John published two milestone papers on PCs in 1988. Before that Lord Rayleigh started his study in 1888, by showing that such systems have a 1D PBG, a spectral range of large reflectivity, known as a stop-band. Further, 1DPCs in the form of periodic multi-layers dielectric stacks (such as the Bragg mirror) are studied extensively. Today, such structures are

used in a diverse range of applications such as reflective coatings for enhancing the efficiency of Light Emitting Diodes (LEDs) and highly reflective mirrors in certain laser cavities.

In 1987, Yablonovitch and John have proposed 2DPCs and 3DPCs, which have a periodic dielectric structure in two dimensions and three dimensions, respectively. The periodic dielectric structures exhibit a PBG. Both of their proposals are concerned with higher dimensional (2D or 3D) periodic optical structures. Yablonovitch's main motivation is to engineer the photonic density of states, in order to control the spontaneous emission of materials that are embedded within the PC. In the similar way, John's idea is to affect the localization and control of light inside the periodic PC structure. Both of these works addresses the engineering of a structured material exhibiting ranges of frequencies at which the propagation of electromagnetic waves is not allowed, so called PBGs - a range of frequencies at which light cannot propagate through the structure in any direction.

After 1987, the number of research papers concerning PCs has begun to grow exponentially. However, owing to the fabrication difficulties of these structures at optical scales, early studies are either theoretical or in the microwave and optical regime, where PCs can be built on the far more readily accessible nanometer scale. By 1991, Yablonovitch has demonstrated the first 3D PBG in the microwave regime.

In 1996, Thomas Krauss made the first demonstration of a 2DPC at optical wavelengths. This opened up the modern way of fabricating PCs in semiconductor materials by the methods used in the semiconductor industry. Although such techniques are still to mature into commercial applications, 2DPCs have found commercial use in the form of Photonic Crystal Fibers (PCFs) and optical components. Since 1998, the 2DPCs based optical components such as optical filters [3,4], multiplexers [5], demultiplexers [6], switches [7], directional couplers [8], power dividers/splitters [9], sensors [10,11] etc., are designed for commercial applications.

3. Types of photonic cyrstals

PCs are classified mainly into three categories according to its nature of structure periodicity, that is, One Dimensional (1D), Two Dimensional (2D), and Three Dimensional (3D) PCs. The geometrical shape of 1DPCs, 2DPCs and 3DPCs are shown in Figure 1 where the different colors represent material with different dielectric constants. The defining structure of a PC is the periodicity of dielectric material along one or more axis. The schematic illustrations of 1DPCs, 2DPCs and 3DPCs are depicted in Figures 2(a), 2(b) and 2(c), respectively.

3.1. One dimensional PCs

In 1DPCs, the periodic modulation of the refractive index occurs in one direction only, while the refractive index variations are uniform for other two directions of the structure. The PBG appears in the direction of periodicity for any value of refractive index contrast i.e., difference between the dielectric constant of the materials. In other words, there is no threshold for dielectric contrast for the appearance of a PBG. For smaller values of index contrast, the width

http://dx.doi.org/10.5772/54533

of the PBG appears very small and vice versa. However, the PBGs open up as soon as the refractive index contrast is greater than one ($n_1/n_2 > 1$), where n_1 and n_2 are the refractive index of the dielectric materials. A defect can be introduced in a 1DPCs, by making one of the layers to have a slightly different refractive index or width than the rest. The defect mode is then localized in one direction however it is extended into other two directions. An example for such a 1DPC is the well known dielectric Bragg mirror consisting of alternating layers with low and high refractive indices, as shown in Figure 2(a).

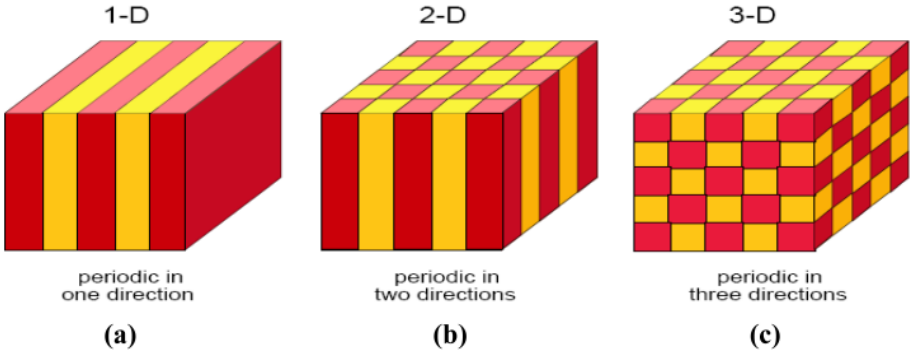

Figure 1. Geometrical shapes of photonic crystals (a) 1D (b) 2D and (c) 3D

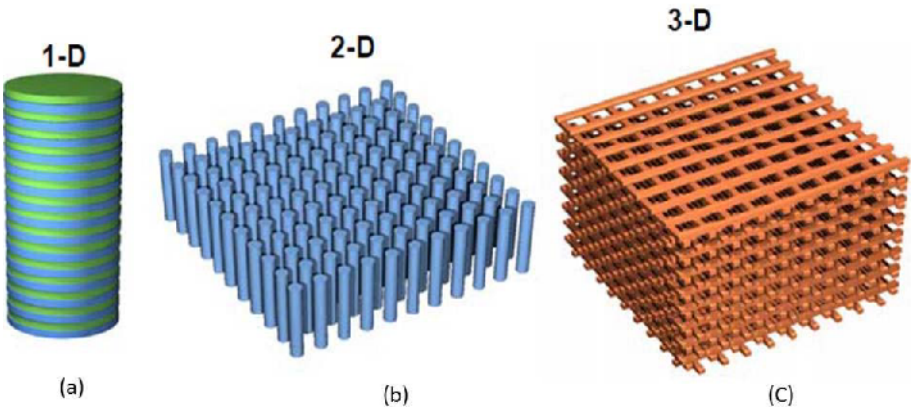

Figure 2. Schematic illustrations of photonic crystals (a) 1D (b) 2D and (c) 3D

The wavelength selection and reflection properties in 1DPCs are used in a wide range of applications including high efficiency mirrors [12,13], optical filters [14,15, 16], waveguides [17], and lasers [18]. Also, such structures are widely used as anti-reflecting coatings which dramatically decrease the reflectance from the surface and used to improve the quality of the lenses, prisms and other optical components.

3.2. Two dimensional PCs

PC structure(s) that are periodic in two different directions and homogeneous in third direction are called 2DPC which is shown in Figure 1.(b) and 2(b). In most of the 2DPCs, the PBG occurs when the lattice has sufficiently larger index contrast. If the refractive index contrast between the cylinders (rods) and the background (air) is sufficiently large, 2D PBG can occur for propagation in the plane of periodicity perpendicular to the rod axis.

Generally, 2DPCs consist of dielectric rods in air host (high dielectric pillars embedded in a low dielectric medium) or air holes in a dielectric region (low dielectric rods in a connected higher dielectric lattice) as shown in Figures 3(a) and 3(b). The dielectric rods in air host give PBG for the Transverse Magnetic (TM) mode where the E field is polarized perpendicular to the plane of periodicity. The air holes in a dielectric region give (Transverse Electric) TE modes where H field is polarized perpendicular to the plane of periodicity.

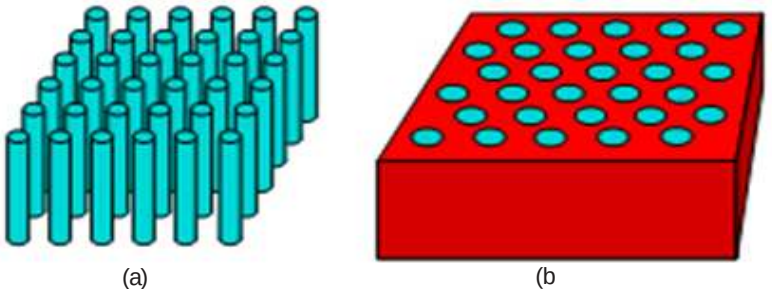

Figure 3. Structure of (a) dielectric rods in air and (b) air holes in dielectric region

Based on the value of vertical index contrast the structures can have, they are categories into the following four geometries:

- Membrane Holes : Hole type PCs with a high vertical index contrast
- Membrane Pillars : Pillar based PCs with a high vertical index contrast
- Deeply etched Holes : Hole type PCs with a low vertical index contrast
- Deeply etched Pillars : Pillar based PCs with a low vertical index contrast

Above all, the membrane holes and pillars with high vertical index contrast received a crucial role for device realization.

3.3. Three Dimensional PCs

A 3DPCs is a dielectric structure which has periodic permittivity modulation along three different axes, provided that the conditions of sufficiently high dielectric contrast and suitable periodicity are met, a PBG appears in all directions. Such 3D PBGs, unlike the 1D and 2D ones,

http://dx.doi.org/10.5772/54533

can reflect light incident from any direction. In other words, a 3D PBG material behaves as an omnidirectional high reflector. As an example, Figure 4 depicts the 3D woodpile structure.

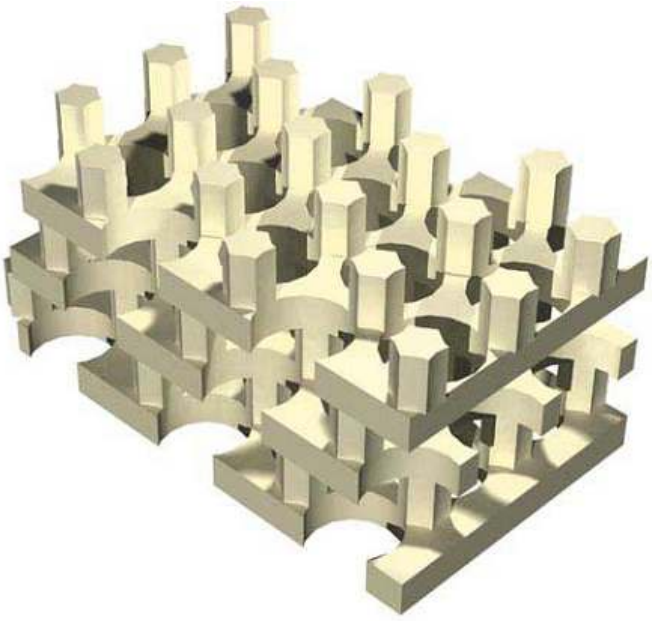

Figure 4. Structure of 3D woodpile photonic crystals

Due to the challenges involved in fabricating high-quality structures for the scale of optical wavelengths, early PCs are performed at microwave and mid-infrared frequencies [19, 20]. With the improvement of fabrication and materials processing methods, smaller structures have become feasible, and in 1999 the first 3DPC with a PBG at telecommunications frequencies is reported [21, 22]. Since then, various lattice geometries have been reported for operation at similar frequencies [23, 24]. Waveguide and the introduction of intentional defects in 3DPCs has not progressed as rapidly as in 2DPCs, due to the fabrication difficulties and the more complex geometry required to achieve 3D PBGs.

4. Numerical analysis

There are many methods available to analyze the dispersion behavior and transmission spectra of PCs such as Transfer Matrix Method (TMM) [25], FDTD method [26], PWE method [27], Finite Element Method [28] (FEM) etc.,. Each method has its own pros and cons. Among these, PWE and FDTD methods are dominating with respect to their performance and also meeting the demand required to analyze the PC based optical devices.

The PWE method is initially used for theoretical analysis of PC structures, which makes use of the fact that Eigen modes in periodic structures can be expressed as a superposition of a set of plane waves. Although this method can obtain an accurate solution for the dispersion properties (propagation modes and PBG) of a PC structure, it has still some limitations. i.e., transmission spectra, field distribution and back reflections cannot be extracted as it considers only propagating modes. An alternative approach which has been widely adopted to calculate both transmission spectra and field distribution is based on numerical solutions of Maxwell's equations using FDTD method. Typically, the PWE method is used to calculate the PBG and propagation modes of the PC structure and FDTD is used to calculate the spectrum of the power transmission.

5. Applications of 2DPCs

The ability to control and manipulate the spontaneous emission by introducing defects in PCs, and related formation of defect state within PBG has been used for designing the optical devices for different applications that are directed towards the integration of photonic devices. 2DPCs is the choice of great interest for both fundamental and applied research, and also it is beginning to find commercial applications. K. Inoue et al 2004 have summarized the use PCs in various applications as shown in Figure 5.

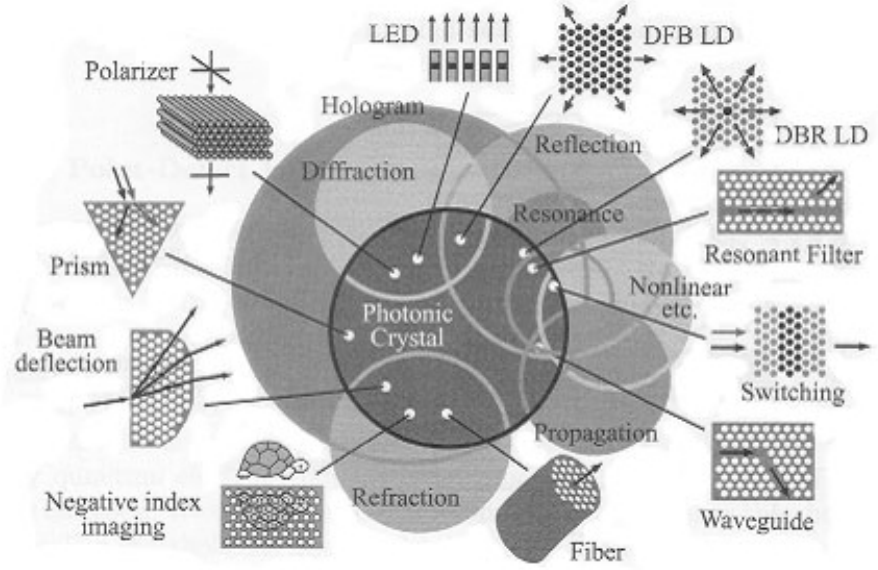

Figure 5. Applications of photonic crystals

The majority of PC applications utilize the phenomenon of PBG that opens the new road to design optical components in micrometer (μm) range. Waveguides that confine light via PBGs are a new development. Generally, the waveguide is intended to transport waves of a particular frequency from one place to another place through a curved path. Using this waveguide many optical components are reported in the literature such as power splitter/ power divider [29] which divides the power in an input waveguide equally between output waveguides, Y splitter [30], and directional couplers [31] and so on.

It is also possible to design a cavity, formed by the absence of a single rod or group of rods (point defects), which is positioned between two waveguides each of which is formed by the absence of a row of rods (line defects). Various geometries of the micro cavities have been explored over the years with a goal of increasing the Q factor of a cavity, while reducing the cavity size. Two main cavity geometries can be distinguished as those are based on point defect based cavity [32] and line/point defect (PCRR) based cavities [33]. Such a cavity is useful for optical filters [34], lasers [35], multiplexers and demultiplexers [36] etc,.

6. Optical ring resonator

An optical ring resonator is positioned between two optical waveguides to provide an ideal structure of the ring resonator based ADF. At resonant condition, the light (signal) is dropped from the bus (top) waveguide and it is sent to the dropping (bottom) waveguide through ring resonator. The schematic structure of the ring resonator based ADF is shown in Figure 6, which consists of a bus waveguide and dropping waveguide, and ring resonator. The ring resonator acts as a coupling element between the waveguides. Also, it has four ports, ports 1 and 2 are the input terminal and transmission output terminals whereas ports 3 and 4 are forward and backward dropping terminals, respectively.

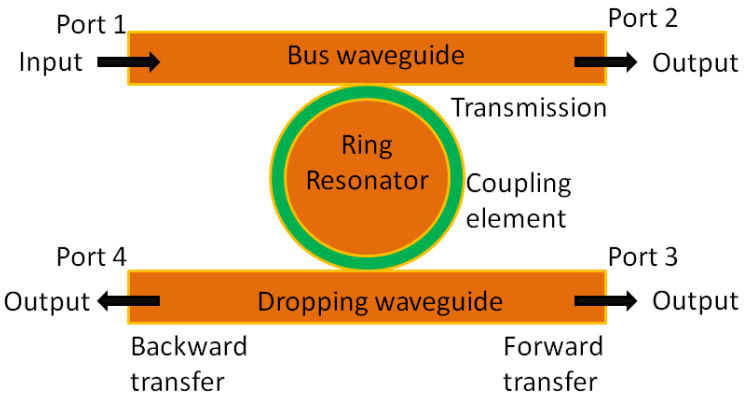

Figure 6. Schematic structure of the ring resonator based ADF

In PC structures, there are two ways to design optical resonator as follows,

i. Line defect or point defect based resonators - changing the size or dielectric constant of rods in the structure

ii. Ring Resonators (RRs) - removing some rods in order to have a ring shape

In RR based devices, the choice of the ring size is determined by the desired resonant wavelength and the tradeoff between the cavity Q and the modal volume V [34]. Compared to point defect or line defect PC cavities, Photonic Crystal Ring Resonators (PCRRs) offer scalability in size, flexibility in mode design due to their multi mode nature [37], easy integration with other devices and adaptability in structure design.

6.1. Operating principle

If the ring resonator supports only one resonant mode, it will decay through both waveguides along the forward and backward directions which introduces the reflection. Hence, in order for complete transfer to happen, at least two modes are needed for the decaying amplitudes to cancel either the backward direction or the forward direction of the bus waveguide (Fan et al 1998).

Two mirror planes can be considered for this structure, one is perpendicular to the waveguides and another is parallel to the waveguides. In order to cancel the reflected signal, a structure with a mirror plane symmetry perpendicular to both waveguides is considered. Assume that there exist two localized modes that have different symmetries with respect to the mirror plane: one has even symmetry and another has odd symmetry. The even mode decays with the same phase into the forward and backward directions as shown in Figure 7(a), however the odd mode decays into the forward direction, out of phase with the decaying amplitude along the backward direction as shown in Figure 7(b). When the two tunneling processes come together, the decaying amplitudes into the backward direction of both waveguides are canceled, which clearly depicts in Figure 7(c). It should be noted that, in order for cancellation to occur, the line shapes of the two resonances should overlap. It means both resonances must have significantly the same resonant wavelength and the same bandwidth [32].

Also, due to the occurrence of degeneracy, the incoming wave interferes destructively with the decaying amplitude into the forward direction of the bus waveguides, causing all the power traveling in the bus waveguide to be cancelled. The symmetry of the resonant modes with respect to the mirror plane parallel to the waveguides determines the direction of the transfer wave in the ADF. For instance, as it apparent from Figures 8(a), 8(b) and 8(c), when both of the modes are even with regard to the parallel mirror plane, the decaying amplitudes along the backward direction of the drop waveguide would be canceled, letting all the power be transferred into the forward direction of the drop waveguide. On the other hand, the even mode could be odd with respect to the mirror plane parallel to the waveguides. When the accidental degeneracy between the states occurs, the decaying amplitudes cancel in the forward direction of the drop waveguide (Figures 8(a), 8(b) and 8(c)). Entire power is transferred into the backward direction of the drop waveguide [32].

http://dx.doi.org/10.5772/54533

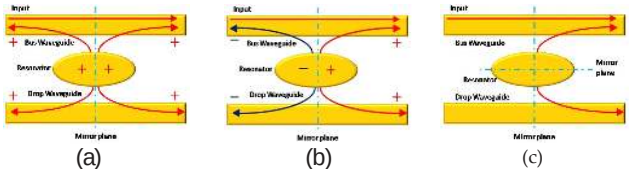

Figure 7. Channel drop tunneling process for a resonator system that supports forward transfer of signal

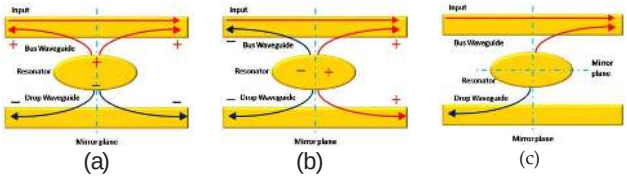

Figure 8. Channel drop tunneling process for a resonator system that supports backward transfer of signal

The PCRR resonant coupling occurs due to the frequency and phase matching between the propagating waveguide mode and the PCRR resonant cavity mode. The coupling direction is mainly determined by the modal symmetry and the relative coupling between the PCRRs. The direction is the same for the propagating wave in the waveguide and the coupled wave inside PCRR. However, the direction may be the same or reverse for the coupling between PCRRs, depending upon the coupling strength and the modal symmetry [32]. Both forward dropping and backward dropping can be obtained depending upon the mode symmetry properties with respect to the coupling configurations.

6.2. Requirements of the ADF

The filter performance is determined by the transfer efficiency between the two waveguides. Perfect efficiency corresponds to complete transfer of the selected channel in either forward or backward direction in the dropping waveguide without forward transmission or backward reflection in the bus waveguide. All other channels remain unaffected by the presence of optical resonators.

To achieve complete transfer of the signal at resonance, the PCRR based ADF must satisfy the following three conditions:

i. The resonator must possess at least two resonant modes, each of them must be even and odd, with respect to the mirror plane of symmetry perpendicular to the waveguides

ii. The modes must degenerate

iii. The modes must have equal Q

All three conditions are necessary to achieve complete transfer of the signal from the bus waveguide to PCRR and PCRR to drop waveguides.

7. Photonic crystal ring resonator based ADF

The PCRR based ADF is designed using two dimensional pillar type PC with circular rods and consists of an array of rods in square lattice, as shown in Figure 9(a). The number of rods in 'X' and 'Z' directions is 21. The distance between the two adjacent rods is 540 nm, which is termed as lattice constant, 'a'. The Si rod with refractive index 3.47 is embedded in the air. The radius of the rods is 0.1 μm and the overall size of the device comes around 11.4 μm × 11.4 μm. The band diagram in Figure 9(b) gives the propagation modes and PBG of the PC structure, which has TM PBG ranging from 0.295 a/λ to 0.435 a/λ whose corresponding wavelength lies between 1241 nm and 1830 nm. It covers the entire wavelength range of third optical communication window. The guided modes (even and odd) inside PBG region resulting due to line and point defects (21×21 PC) are shown in Figure 9(c) which supports the complete channel transfer in turn higher output efficiency at resonance. The structure is surrounded by Perfect Matched Layer (PML) as absorbing boundary conditions to truncate the computational regions and to avoid the back reflections from the boundary [38].

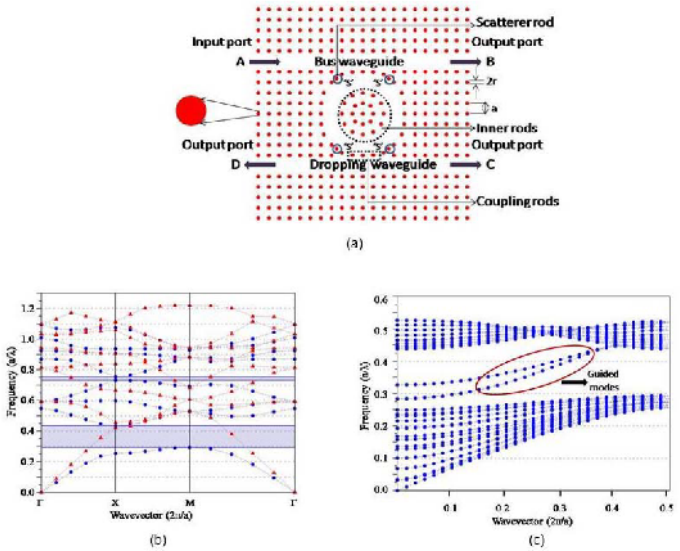

Figure 9. a) Schematic structure of circular PCRR based ADF (b) band diagram of 1 × 1 PC (unit cell) and (c) band diagram of 21 ×2 1 PC (super cell) structure after the introduction of line and point defects

The normalized transmission spectra of the circular PCRR based ADF is obtained using 2D Finite Difference Time Domain (FDTD) method. Although the real SOI structure, would, in

practice, require 3D analysis, our 2D approach gives a general indication of the expected 3D behavior. 2D analysis carried out here allows us to identify qualitatively many of the issues in the cavity design (e.g. mode control, cavity Q and the placement of the scatterers in our quasi-square ring cavity) and the coupling scheme design. This can offer us the design trade-offs and guidelines before the real structure design based on a completely 3D FDTD technique, which is typically computational time and memory consuming.

The circular PCRR based ADF (in Figure 9 (a)) consists of two waveguides in horizontal (r-x) direction and a circular PCRR is positioned between them. The top waveguide is called as bus waveguide whereas the bottom waveguide is known as dropping waveguide. The input signal port is marked 'A' with an arrow on the left side of bus waveguide. The ports 'C' and 'D' of drop waveguide is the drop terminals and denoted as forward dropping and backward dropping, respectively, while the port 'B' on the right side of bus waveguide is designated as forward transmission terminal.

The bus and the dropping waveguides are formed by introducing line defects whereas the circular PCRR is shaped by creating point defects (i.e. by removing the columns of rods to make a circular shape). The circular PCRR is constructed by varying the position of inner rods and outer rods from their original position towards the center of the origin (r). The inner rods are built by varying the position of adjacent rods on the four sides, from their center, by 25%, on the other hand the outer rods are constructed by varying the position of the second rod on the four sides, from their center, by 25% in both 'X' and 'Z' directions. The number of rings that are formed by the ring is three. In order to improve the coupling efficiency, dropping efficiency and spectral selectivity by suppressing the counter propagation modes, the scatterer rods (labeled as 's') are placed at each corner of the four sides with half lattice constant. The material properties and dimension of the scatterer rods are similar to the other rods. The rods which are located inside the circular PCRR are called inner rods whereas the coupling rods are placed between circular PCRR and waveguides. At resonance, the wavelength is coupled from the bus waveguide into the dropping waveguide and exits through one of the output ports. The coupling and dropping efficiencies are detected by monitoring the power at ports 'B' and, 'C' and 'D', respectively.

A Gaussian input signal is launched into the input port. The normalized transmission spectra at ports 'B', 'C' & 'D' are obtained by conducting Fast Fourier Transform (FFT) of the fields that are calculated by 2D-FDTD method. The input and output signal power is recorded through power monitors by placing them at appropriate ports. The normalized transmission is calculated through the following formula:

$$T(f) = \frac{1 \Big/ 2 \int real(p(f)^{monitor}) dS}{Source\ Powe}$$

where T(f) is normalized transmission which is a function of frequency, p(f) is poynting vector and dS is the surface normal. The normalization at the output side does not affect the result because of source power normalization. Finally, the T(f) is converted as a function of wavelength.

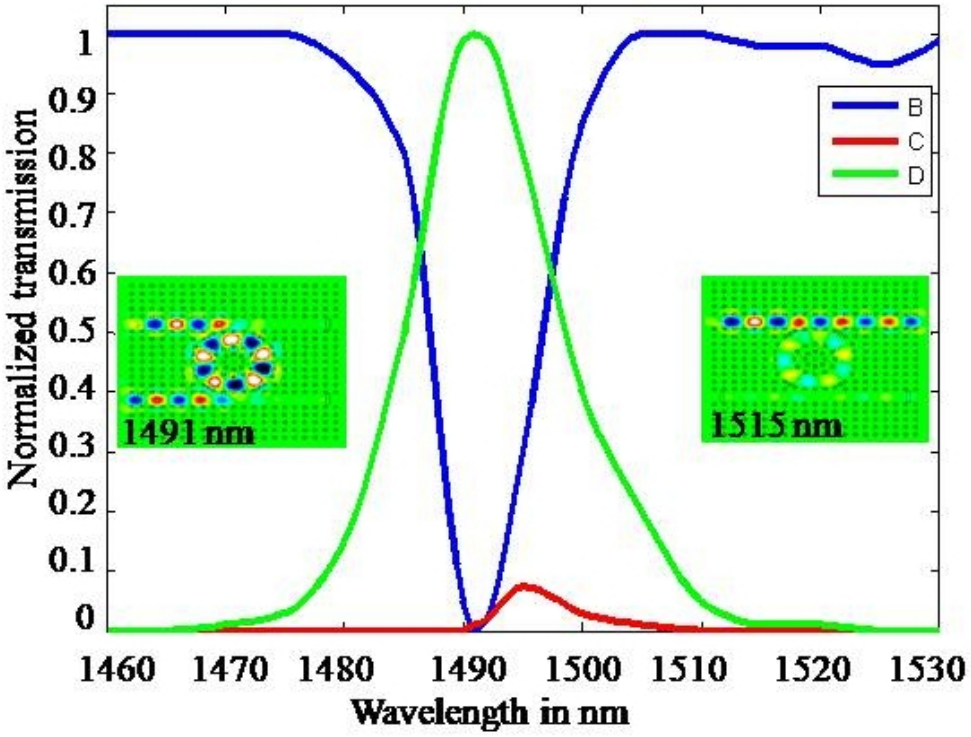

Figure 10. Normalized transmission spectra of circular PCRR based ADF

Figure 10 shows the normalized transmission spectra of circular PCRR based ADF. The resonant wavelength of the ADF is observed at 1491 nm. The simulation shows 100% coupling and dropping efficiencies and its passband width is 13 nm. The Q factor, which is calculated as $\lambda/\Delta\lambda$ (resonant wavelength/full width half maximum), equals to almost 114.69. The obtained results meet the requirements of ITU-T G 694.2 CWDM systems. The inset in Figure 10 depicts the electric field pattern of pass and stop regions at 1491 nm and 1515 nm, respectively. At a resonant wavelength, λ=1491 nm the electric field of the bus waveguide is fully coupled with the ring and reached into its output port D. In this condition there is no signal flow in port B. Similarly, at off resonance, λ=1515 nm the signal directly reaches the transmission terminal (the signal is not coupled into the ring). Figure 11 clearly illustrates the three dimensional view of PCRR based ADF. It shows the arrangement of Si rods in the structure and the overall dimensions of the device would come around 11.4 μm (length) × 11.4 μm (width). The effect of point to point network after incorporating the PCRR based ADF is discussed in the following sections.

http://dx.doi.org/10.5772/54533

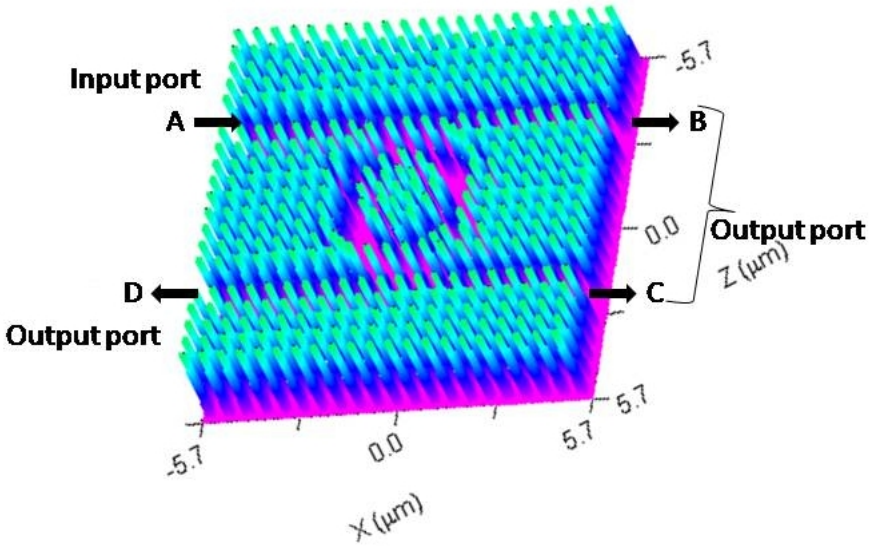

Figure 11. Three dimensional view of circular PCRR based ADF

7.1. Tuning of Resonant Wavelength

Although the PCRR based ADFs have a fixed operating wavelength, the application area will become much broader if the operating wavelength can be tuned dynamically and externally. This would greatly improve the utilization of PC based optical devices for real time and on demand applications. Generally, the resonant wavelength tuning of PCRR based ADF can be done by altering the structural parameters such as refractive index (dielectric constant), lattice constant and radius of the rods in the structure. Among these, the most efficient way to tune the resonant (operating) wavelength of the ADF is changing the refractive index of the material since it is not resulting in degradation of filter performance. Recent year, the exploration of tunablity for 2D PC based optical devices is mainly being carried out with respect to the refractive index [39, 40], lattice constant [41] and radius of the rod [42]. There are several tuning mechanisms such as thermal tuning [39], mechanical tuning [42, 43], MEMS actuator [44] etc., are reported to change the structural parameters. Here, the changes in refractive index, the radius of the rod and lattice constant are considered to examine the possibility of resonant wavelength tuning.

The normalized transmission spectra with respect to the refractive index difference, radius of the rod and lattice constant are shown in Figures 12 (a), (b) and (c), respectively. All the three cases, while varying the structural parameters the coupling and dropping efficiencies are not changing however there is a trivial change in passband width in turn Q factor.

It is observed that, while increasing (decreasing) the value of refractive index, lattice constant and radius of the rod, the resonant wavelength of the filter shifts into the longer wavelength

(shorter wavelength). However, the other filter parameters such as coupling efficiency, dropping efficiency and Q factor are not affected while changing the refractive index and radius of the rod. There is a significant change is observed while varying the lattice constant.

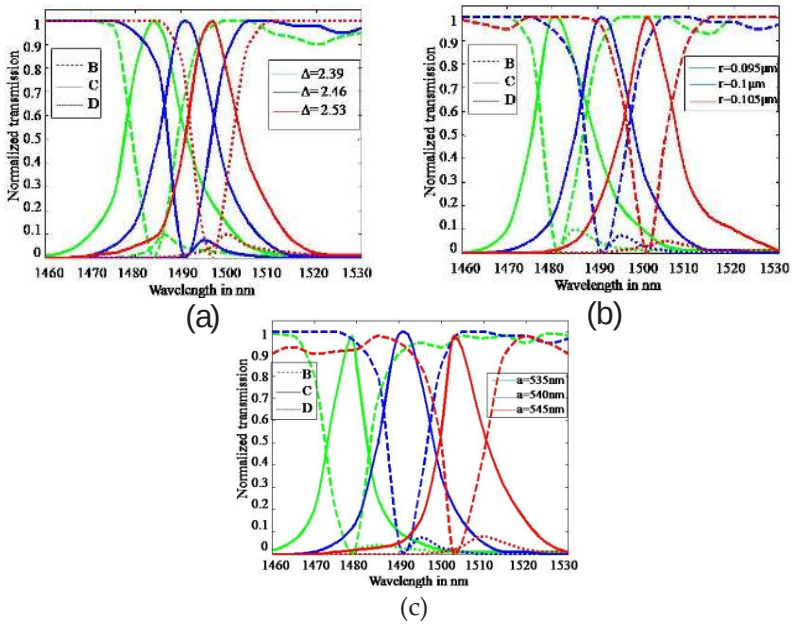

Figure 12. The effect of normalized transmission spectra of the circular PCRR based ADF for varying : (a) refractive index difference (b) radius of the rod and (c) lattice constant

Further, to investigate the impact of resonance for small variation in structural parameters, the simulation is carried out with very small step value. The accounted step value for refractive index difference, radius of the rod and lattice constant is 0.01, 0.001 μm and 1 nm, respectively whose corresponding resonant wavelength shift is shown in Figure 13(a). While considering the change in refractive index, other two parameters are kept constant and vice versa. The shift in resonant wavelength for an infinitesimal change in the refractive index, radius of the rods and lattice constant is given below:

$\Delta\lambda / \Delta n$ = 1 nm / 0.01 (for refractive index difference)

$\Delta\lambda / \Delta r$ = 2 nm / 0.001 μm (for radius of the rods)

$\Delta\lambda / \Delta a$ = 2.2 nm / 1 nm (for lattice constant)

where $\Delta\lambda$ is the shift in resonant wavelength, Δn is the change in refractive index difference, Δr is the change in radius of the rod and Δa is the change in lattice constant. It means that there

is 1 nm shift in resonant wavelength for every change in 0.01 values of the refractive index difference.

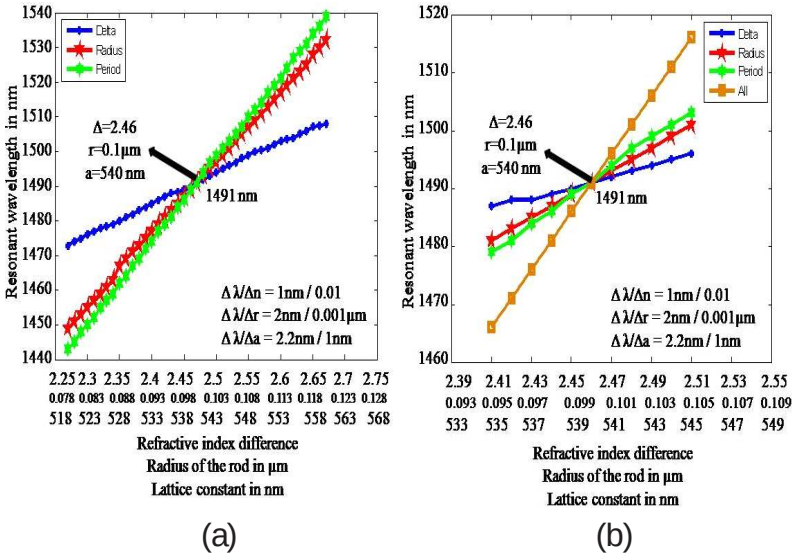

Figure 13. Effect of resonant wavelength shift with respect to refractive index difference, radius of the rod and lattice constant (a) individually and (b) combinedly

The wide tuning range (1471 nm to 1611 nm) is possible by altering any one of the structural parameters. If we considered only one parameter to arrive wide tuning range, the required change in parameter is large which affects the filter parameters. It can be figured out by varying all the structural parameters simultaneously instead of changing any one of the parameters. As expected, there is 5.2 nm resonance shift observed while simultaneously changing the refractive index difference, radius of the rod and lattice constant by 0.01, 0.001 μm and 1 nm, respectively, from the reference value. As discussed earlier, for every change in 0.01 refractive index, 0.001μm radius of the rod and 1 nm lattice constant, there is 1 nm, 2 nm and 2.2 nm resonant wavelength shift is observed. If there is a uniform step change in all the parameters, the cumulative individual resonance shift of (1nm+2nm+2.2nm) 5.2 nm is noted, which is shown in Figure 13(b).

8. BPF using quasi-waveguides

In Wavelength Division Multiplexing (WDM) systems, the number of incoming channels are departed into an optical fiber with designated wavelengths. Hence, optical filters are necessary

to select a required channel(s) at any destination. The BPF is a right device to select either a single or multiple channels from the multiplexed signals. In the literature, PC based BPF has been designed by introducing point defects and/or line defects [44, 45], using bi-periodic structures [46] and using liquid crystal photonic bandgap fibers [47]. Moreover, no other methods are reported to design PC based BPF. The circular PCRR based BPF is designed by exploiting the coupling between the quasi-waveguides and circular PCRR and its simulation results are presented.

8.1. Design of the structure

The structural parameters such as radius of the rod (0.1μm), lattice constant (540 nm), and refractive index (3.46) are chosen to be similar to the previous one. However, the total number of rods in the structure in 'X' and 'Z' directions is 21 and 19, respectively. As the basic structure (rods in air) and its parameters are similar to previous one, therefore, the PBG ranges are also similar.

Figure 14 sketches the schematic structure of the circular PCRR based BPF. The BPF consists of two quasi waveguides in horizontal (r-x) direction and a circular PCRR between them. The Gaussian signal is applied to the port marked 'A' (arrow in the left side of top quasi waveguide) and the output is detected using power monitor which is positioned at the output port marked 'B' (arrow left side of the bottom quasi waveguide). The coupling rod is placed between circular PCRR and quasi waveguides, marked as 'c'. The reflectors, demarcated in a rectangular box, placed above and below the right side of circular PCRR are shown in Figure 14, which are used to improve the output efficiency of the BPF by reducing the counter propagation modes. In order to enhance the output efficiency and maintain the structure in symmetric nature, the number of periods (Si rods) in the reflector is kept constant, 9.

The structural parameters such as radius of the rod (0.1μm), lattice constant (540 nm), and refractive index (3.46) are chosen to be similar to the previous one. However, the total number of rods in the structure in 'X' and 'Z' directions is 21 and 19, respectively. As the basic structure (rods in air) and its parameters are similar to previous one, therefore, the PBG ranges are also similar.

Figure 14 sketches the schematic structure of the circular PCRR based BPF. The BPF consists of two quasi waveguides in horizontal (r-x) direction and a circular PCRR between them. The Gaussian signal is applied to the port marked 'A' (arrow in the left side of top quasi waveguide) and the output is detected using power monitor which is positioned at the output port marked 'B' (arrow left side of the bottom quasi waveguide). The coupling rod is placed between circular PCRR and quasi waveguides, marked as 'c'. The reflectors, demarcated in rectangular box, placed above and below the right side of circular PCRR are shown in Figure 14, which are used to improve the output efficiency of the BPF by reducing the counter propagation modes. In order to enhance the output efficiency and maintain the structure in symmetric nature, the number of periods (Si rods) in the reflector is kept constant, 9.

http://dx.doi.org/10.5772/54533

8.2. Simulation results and discussion

The normalized transmission spectra of PCRR based BPF are shown in Figure 15(a). The observed output efficiency is approximately 85% at 1420 nm and close to 100% over the range of wavelengths 1504 nm to 1521 nm whose corresponding bands are denoted as Band I and Band II, respectively. The center wavelength and FWHM bandwidth of these bands are 1420 nm and 1512.5 nm, and 20 nm and 35 nm, respectively. Also, the calculated Q factor of Band I and Band II is 71 and 50.41, respectively. As it is witnessed, the number of passbands depends on the number of inner rings that are formed by the inner rods. Here, the two inner rings considered results in two passbands. The size and shape of the ring resonator determines the resonant wavelength. The bandwidth and channel spacing are decided by the other structural parameters namely, radius of the rod, period and dielectric constant (refractive index) of the material.

The Figure 15(b) illustrates the relation between the output efficiency and wavelength shift for different dielectric constant of the structure. It can be seen clearly that the center wavelength of the bands shifts into the lower wavelength region when the dielectric constant of structure is decreased, and similarly the center wavelength of the bands shifts into the higher wavelength region when the dielectric constant of the structure is increased. It is also noticed that the output efficiency is not significantly changed while varying the dielectric constant of the structure. The magnitude of the wavelength shift is around 9 nm for every 0.5 change in dielectric constant value of the structure. However, the bandwidth is almost not affected by the variation of dielectric constant.

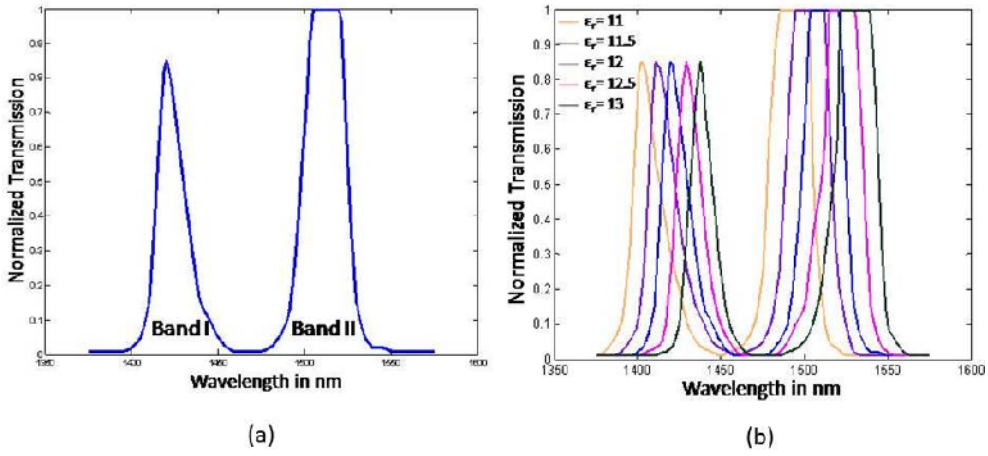

Figure 15. Normalized transmission spectra of (a) circular PCRR based BPF and (b) for different values of dielectric constant

9. PCRR based BSF

Essentially, BSF is one of the prominent components to suppress (remove) either single or multiple unwanted channels from the multiplexed output channels, or also it passes most of the frequency range unaltered, however it attenuates/stops a specific range. In literature, the PC based BSF have been designed by introducing point and line defects [49], and using square and rectangular resonant cavity [50]. As the cavity size is small in the defects based BSFs, it does not provide the wide stopband width even it has higher stopband efficiency. Though, the square and rectangular cavities based BSFs offers a wide stopband width, it reduces the stopband efficiency owing to scattering at corners in resonance condition as it has proper corner. The proposed circular PCRR has gradual changes at corner and subtle in nature which is considered here for designing BSF.

9.1. Design of the structure

The proposed BSF is designed using 2D square lattice PCs with circular PCRR, which is shown in Figure 16. The number of rods in 'X' and 'Z' directions (21), lattice constant (540 nm), radius of the rod (0.1 μm) and refractive index of the rods (3.46) are similar as the filters discussed in the previous chapters. The PCRR based BSF, consists of a waveguide in horizontal (r-x) direction and a circular PCRR below the waveguide. The waveguide is called as bus waveguide and the ring resonator has 4 rings of Si rods in the inner rods (cavity). The bus waveguide is formed by introducing line defects and the circular PCRR is shaped by point defects.

The circular PCRR consists of four rings in the inner cavity, which is constructed by varying the position of both inner and outer rods from their original position towards center of the origin (r). In the four rings inner cavities, the center rod in the structure is considered as the first ring and the second ring is placed around the first ring and then third ring followed by the fourth ring. The inner rods are built by varying the position of adjacent rods in the four sides, from their center, by 25%, whereas the outer rods are constructed by varying the position of the second rod on four sides, from its center, by 25% both in 'X' and 'Z' directions where 'X' is the horizontal direction and 'Z' is the vertical direction. The position of the rods is varied by varying the lattice constant.

At resonance, the signal is coupled into the PCRR from bus waveguide and reflected back to the input port, hence the signal is not reached into the output at that resonant condition. This behavior is used to stop single or multiple channels from the multiplexed input/output channels. The stopband efficiency is obtained by monitoring the power at port 'B' at resonant condition.

Figure 17 shows the normalized transmission spectra of PCRR based BSF. The stopband efficiency of the BSF is approximately 98% and the width of the stopband is 11 nm. Here, the stopband width is calculated at FWHM point and the stopband efficiency is computed by subtracting the detected output power from the normalized transmission value and multiplying by 100.

http://dx.doi.org/10.5772/54533

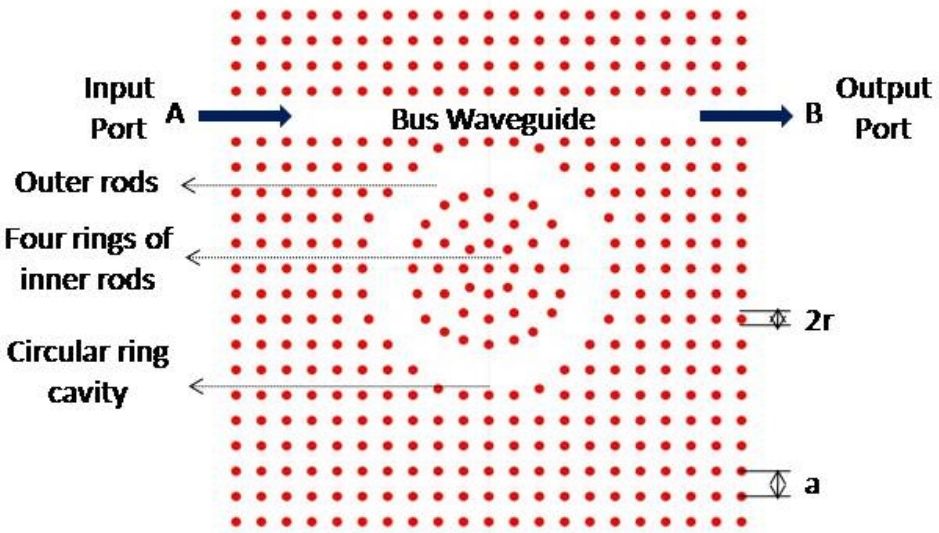

Figure 16. Schematic structure of circular PCRR based BSF

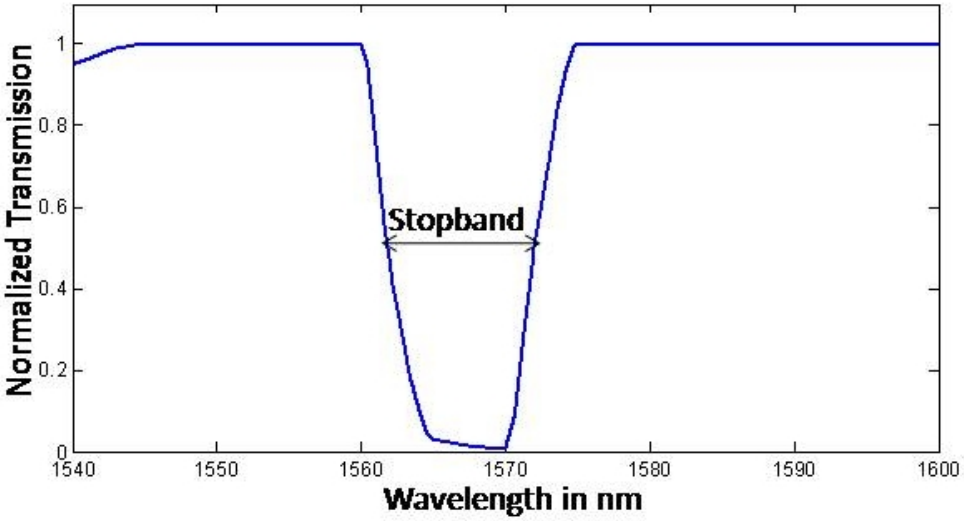

Figure 17. Normalized transmission spectra of circular PCRR based BSF

The Figures 18(a) and 18(b) depict the typical electric field pattern for pass and stop bands at 1550 nm and 1570 nm, respectively. At resonant wavelength, λ=1550 nm the electric field of

the bus waveguide is fully transferred to the output port (OFF resonance), and hence, the maximum transfer efficiency is obtained, whereas at 'ON' resonance, λ=1570 nm the signal is coupled into the resonant cavity from the bus waveguide and reflected back to the input. Hence, the signal does not reach the output port which reduces the output power.

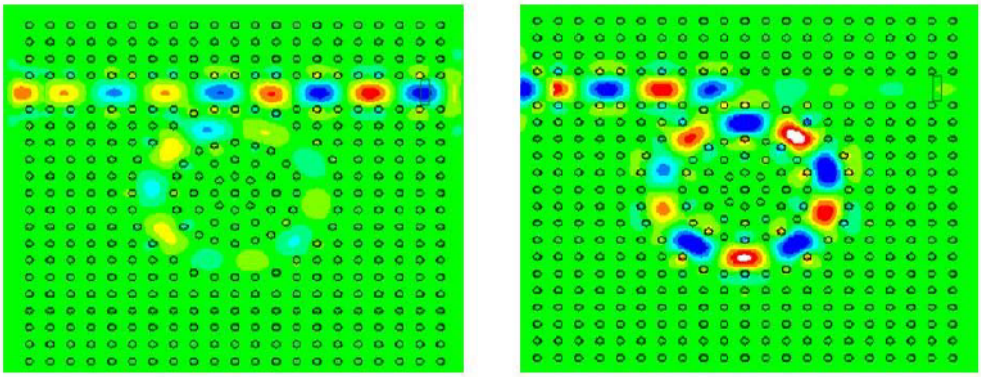

Figure 18. Electric field pattern of the circular PCRR based BSF at: (a) 1550 nm and (b) 1570nm

10. Conclusion

In this Chapter, we have reviewed the progress of photonic crystal ring resonators and ring resonator devices. Emphasis has been on the principles and applications of ultra-compact photonic crystal ring resonators. We proved that circular PCRR based optical filters provide better performance than others. These findings make the PCRRs an alternative to current microring resonators for ultra-compact WDM components and applications in high-density photonic integration.

Author details

S. Robinson* and R. Nakkeeran

*Address all correspondence to: mail2robinson@pec.edu

Department of Electronics, School of Engineering and Technology, Pondicherry University, Puducherry, India

References

[1] Yablonovitch, E. (1987). Inhibited spontaneous emission on solid-state physics and electronics", Physics Review Letters, , 58(20), 2059-2062.

[2] John, S. (1987). Strong localization of photons in certain disordered dielectric superlattices", Physics Review Letters, , 58(23), 2486-2489.

[3] Ma, Z, & Ogusu, K. (2011). Channel drop filters using photonic crystal fabry-perot resonators", Optics Communications, , 284(5), 1192-1196.

[4] Mohmoud, M. Y, Bassou, Z. M, Taalbi, A, & Chekroun, Z. M. (2012). Optical channel drop filters based on photonic crystal ring resonators", Optics Communications, , 285(1), 368-372.

[5] Rawal, S, & Sinha, R. K. (2009). Design, analysis and optimization of silicon-on-insulator photonic crystal dual band wavelength demultiplexer", Optics Communications, , 282(19), 3889-3894.

[6] Benisty, H, Cambournac, C, Laere, F. V, & Thourhout, D. V. (2010). Photonic crystal demultiplexer with improved crosstalk by second-order cavity filtering", Journal of Lightwave Technology, , 28(8), 1201-1208.

[7] Wang, Q, Cui, Y, Zhang, H, Yan, C, & Zhang, L. (2010). The position independence of heterostructure coupled waveguides in photonic-crystal switch", Optik Optics, , 121(8), 684-688.

[8] Moghaddam, M. K, Attari, A. R, & Mirsalehi, M. M. (2010). Improved photonic crystal directional coupler with short length", Photonics and Nanostructures-Fundamentals and Applications, , 8(1), 47-53.

[9] Gannat, G. A, Pinto, D, & Obayya, S. S. A. (2009). New configuration for optical waveguide power splitters", IET Optoelectroncis, , 3(2), 105-111.

[10] Abdel Malek F ((2011). Design of a novel left-handed photonic crystal sensor operating in aqueous environment", IEEE Photonics Technology Letters, , 23(3), 188-190.

[11] Olyaee, S, & Dehghani, A. A. (2012). High resolution and wide dynamic range pressure sensor based on two-dimensional photonic crystal", Photonic Sensors, , 2(1), 92-96.

[12] Bruyant, A, Lerondel, G, Reece, P. J, & Gal, M. (2003). All silicon omnidirectional mirrors based on one-dimensional photonic crystals", Applied Physics Letters, , 82(19), 3227-3229.

[13] Li, Y, Xiang, Y, Wen, S, Yong, J, & Fan, D. (2011). Tunable terahertz mirror and multi channel terahertz filter based on one dimensional photonic crystals containing semiconductors", Journal of Applied Physics, , 110(7), 073111-073111.

[14] Chen, M. C, Luan, P. G, & Lee, C. T. (2003). Novel design of organic one-dimensional photonic crystal filter", in the Proceedings of the 5th IEEE International Conference on Lasers and Electro-Optics, , 2, 1-4.

[15] Nemec, H, Duvillaret, L, Garet, F, Kuzel, P, Xavier, P, Richard, J, & Rauly, D. (2004). Thermally tunable filter for terahertz range based on a one-dimensional photonic crystal with a defect", Journal of Applied Physics, , 96(8), 4072-4075.

[16] Lee, H. Y, Cho, S. J, Nam, G. Y, Lee, W. H, Baba, T, Makino, H, Cho, M. W, & Yao, T. (2005). Multiple wavelength transmission filters based on Si-SiO_2 one dimensional photonic crystals", Journal of Applied Physics, , 97(10), 103111-103111.

[17] Taniyama, H. (2002). Waveguide structures using one-dimensional photonic crystal", Journal of Applied Physics, , 91(6), 3511-3515.

[18] Lu, T. W, Chiu, L. H, Lin, P. T, & Lee, P. T. (2011). One-dimensional photonic crystal nanobeam lasers on a flexible substrate", Applied Physics Letters, , 99(7), 071101-071101.

[19] Ogawa, S, Tomoda, K, & Noda, S. (2002). Effects of structural fluctuations on three dimensional photonic crystals operating at near-infrared wavelengths", Journal of Applied Physics, , 91(1), 513-515.

[20] Yang, Y. L, Hou, F. J, Wu, S. C, Huang, W. H, Lai, M. C, & Huang, Y. T. (2009). Fabrication and characterization of three dimensional all metallic photonic crystals for near infrared applications", Applied Physics Letters, , 94(4), 041122-041122.

[21] Baohua, J, Buso, D, Jiafang, L, & Min, G. (2009). Active three dimensional photonic crystals with high third order nonlinearity in telecommunication", in the Proceedings of the IEEE International Conference on Lasers and Electro Optics, , 1-2.

[22] Deubel, M, Von Freymann, G, Wegener, M, Pereira, S, Busch, K, & Soukoulis, C. M. (2004). Direct laser writing of three dimensional photonic crystal templates for photonic bandgaps at telecommunication wavelengths", in the Proceedings of the IEEE International Conference on Lasers and Electro Optics, , 1-3.

[23] Ohkubo, H, Ohtera, Y, Kawakami, S, & Chiba, T. (2004). Transmission wavelength shift of +36 nm observed with Ta_2O_5-SiO_2 multichannel wavelength filters consisting of three dimensional photonic crystals", IEEE Photonic Technology Letters, , 16(5), 1322-1324.

[24] Liu, R. J, Li, Z. Y, Feng, Z. F, Cheng, B. Y, & Zhang, D. Z. (2008). Channel drop filters in three dimensional woodpile photonic crystals", Journal of Applied Physics, , 103(9), 094514-094514.

[25] Pendry, J. B. and MacKinnon A ((1992). Calculation of photon dispersion relation", Physics Review Letters, , 69(19), 2772-2775.

[26] Taflove, A. (2005). Computational Electrodynamics: The Finite-Difference Time Domain Method", Artech House, Boston, London.

[27] Pendry, J. B. (1996). Calculating photonic band structure", Journal of Physics: Condensed Matter, , 8(9), 1085-1108.

[28] Pelosi, G, Coccioli, R, & Selleri, S. (1997). Quick Finite Elements for Electromagnetic waves", Artech House, Boston, London.

[29] Djavid, M, Ghaffari, A, Monifi, F, & Abrishamian, M. S. (2008). Photonic crystal power dividers using L-shaped bend based on ring resonators", Journal of Optical Society of America B, , 25(8), 1231-1235.

[30] Borel, P. I, Frandsen, L. H, Harpoth, A, Kristensen, M, Jensen, J. S, & Sigmund, O. (2005). Topology optimized broadband photonic crystal Y-splitter", Electronics Letters, , 41(2), 69-71.

[31] Moghaddam, M. K, Attari, A. R, & Mirsalehi, M. M. (2010). Improved photonic crystal directional coupler with short length", Photonics and Nanostructures-Fundamentals and Applications, , 8(1), 47-53.

[32] Fan, S, Villeneuve, P. R, Joannopoulos, J. D, & Haus, H. A. (1998). Channel drop tunneling through localized states", Physics Review Letters, , 80(5), 950-963.

[33] Mai, T. T, Hsiao, F. L, Lee, C, Xiang, W. F, & Chen, C. C. (2011). Optimization and comparison of photonic crystal resonators for silicon microcantilever sensors", Sensors and Actuators A: Physical, , 165(1), 16-25.

[34] Qiang, Z, Zhou, W, & Soref, R. A. (2007). Optical add-drop filters based on photonic crystal ring resonators", Optics Express, , 15(4), 1823-1831.

[35] Siriani, D. F, & Choquette, K. D. (2010). In-phase, coherent photonic crystal vertical cavity surface emitting laser arrays with low divergence", Electronics Letters, , 46(10), 712-714.

[36] Shih, T. T, Wu, Y. D, & Lee, J. J. (2009). Proposal for compact optical triplexer filter using 2-D Photonic crystals", IEEE Photonics Technology Letters, , 21(1), 18-21.

[37] Manolatou, C, Khan, M. J, Fan, S, Villeneuve, P. R, Haus, H. A, & Joannopoulos, J. D. (1999). Coupling of modes analysis of resonant channel add drop filters", IEEE Journal of Quantum Electronics, , 35(9), 1322-1331.

[38] Berenger, J. P. (1994). A perfectly matched layer for the absorption of electromagnetic waves", Journal of Computational Physics, , 114(2), 185-200.

[39] Figotin, A, Godin, Y. A, & Vitebsky, I. (1998). Two-dimensional tunable photonic crystal", Physical Review B, , 57(5), 2841-2848.

[40] Levy, O, Steinberg, B. Z, Boag, A, Krylov, S, & Goldfarb, I. (2007). Mechanical tuning of two-dimensional photonic crystal cavity by micro electro mechanical flexures", Sensors and Actuators A, , 139(1-2), 47-52.

[41] Hadzialic, S, Kim, S, Sarioglu, A. F, Sudbo, A. S, & Solgaard, O. (2010). Displacement sensing with a mechanically tunable photonic crystal", IEEE Photonics Technology Letters, , 22(12), 1196-1198.

[42] Asano, T, Kunishi, W, Nakamura, N, Song, B. S, & Noda, S. (2005). Dynamic wavelength tuning of channel drop device in two dimensional photonic crystal slab", Electronics Letters, , 41(1), 37-38.

[43] Chew, X, Zhou, G, Chaum, F. S, Dens, J, Tang, X, & Loke, Y. C. (2010). Dynamic tuning of an optical resonator through MEMS driven coupled photonic crystal nano cavities", Optics Letters, , 35(15), 2517-2519.

[44] Costa, R, Melloni, A, & Martinelli, M. (2003). Band-pass resonant filters in photonic crystal waveguides", IEEE Photonics Technology Letters, , 15(3), 401-403.

[45] Chao, C, Li, X, Li, H, Xu, K, Wu, J, & Lin, J. (2007). Bandpass filters based on phase-shifted photonic crystal waveguide gratings", Optics Express, , 15(18), 11278-11284.

[46] Djavid, M, Ghaffari, A, Monifi, F, & Abrishamian, M. S. (2008). Photonic crystal narrow band filters using biperiodic structures", Journal of Applied Science, , 8(10), 1891-1897.

[47] Wei, L, Alkeskjold, T. T, & Bjarklev, A. (2010). Electrically Tunable Bandpass Filter on Liquid Crystal Photonic bandgap fibers", in the Proceedings of the international Conference on OFC/NFOEC, , 1-3.

[48] Oswald, J. A, Wu, B. I, Mcintosh, K. A, & Verghese, S. (2000). Metallo-dielectric photonic crystals for infrared applications", in the Proceedings of Quantum Electronics and Laser Science conference, , 42-43.

[49] Djavid, M, Ghaffari, A, Monifi, F, & Abrishamian, M. S. (2008). Photonic crystal narrow band filters using biperiodic structures", Journal of Applied Science, , 8(10), 1891-1897.

[50] Monifi, F, Djavid, M, Ghaffari, A, & Abrishamian, M. S. (2008). A new bandstop filter based on photonic crystals", in the Proceedings of Progress in the Electromagnetic Research, Cambridge, USA, , 674-677.